minerals

Article

Triassic Appinite from the Qinling Orogen (Central China): Hydrous Melting of Depleted Mantle Wedge in Post-Collision Stage

Hang Liu, Hujun Gong *, Fenhong Luo, Yaqin Zhang and Ben Dang

State Key Laboratory of Continental Dynamics, Department of Geology, Northwest University, Xi'an 710069, China
* Correspondence: gonghujun@nwu.edu.cn

Abstract: Mantle wedge melting and the formation of hydrous mafic melts in collision orogenic belts have great significance for crustal melting and the related granitic magmatism, which can provide key messages about the crustal–mantle interaction in the convergent margin. This paper reported Late-Triassic appinite (212 ± 2 Ma), which is closely associated with Late-Triassic granites. The large euhedral hornblende crystals in the appinite indicate a water-rich feature. This appinite displays low SiO_2 (46.55% to 50.44%) contents, high MgO (7.62 to 10.76%) and Cr and Ni contents, with high Mg# values of 61 to 75. It also displays insignificant Eu anomalies (Eu*/Eu = 0.91 to 0.93), high Sr (596 to 676 ppm) contents and moderate Sr/Y (34 to 40) ratios; these features are similar to those of Sanukite formed by the hydrous melting of the mantle wedge. Its depleted zircon Lu-Hf isotopic composition ($\varepsilon_{Hf(t)}$ = +0.97 to +18.21) indicates a depleted mantle source. Zircons in the appinite display extremely high Ti-in zircon temperatures (>1000 °C) and high oxygen fugacity, indicating a high-temperature hydrous condition. In combination with its typical arc-like trace element geochemistry (depletion in Nb, Ta and Ti), it is proposed that this appinite represents hydrous mafic melts that derived from the melting of the depleted sub-arc mantle wedge. The occurrence of this appinite has great significance for the further understanding of Triassic granitic magmatism and potential magmatic metal ore deposits in the Qinling orogenic belt.

Keywords: hydrous mafic melt; mantle wedge; Triassic; qinling orogen; appinite

check for updates

Citation: Liu, H.; Gong, H.; Luo, F.; Zhang, Y.; Dang, B. Triassic Appinite from the Qinling Orogen (Central China): Hydrous Melting of Depleted Mantle Wedge in Post-Collision Stage. *Minerals* **2023**, *13*, 441. https://doi.org/10.3390/min13030441

Academic Editor: Shoji Arai

Received: 28 November 2022
Revised: 23 February 2023
Accepted: 24 February 2023
Published: 20 March 2023

1. Introduction

Intermediate-felsic rocks, especially the granites in the convergent margin, can provide key messages about the crust–mantle architecture and variations in melting regime [1,2]. However, the mafic rocks in the convergent margin have received limited attention [3]. The appintes, firstly discovered in Caledonide orogen [4], represent mafic to ultramafic rocks closely related with coeval high Ba-Sr granites, which are characterized by coarse idiomorphic hornblende grains (>2 mm) as phenocrysts and in the matrix [4,5]. According to their unique geochemical features, i.e., enriched LILEs and LREE, evolved Sr-Nd isotopic compositions are considered to represent hydrous mafic melts derived from the melting of the metasomatized mantle lithosphere. The occurrence of appinites can provide some important information about crustal–mantle interaction and crustal growth in orogenic belts. Several appinites have been reported in some typical orogenic belts, e.g., the Early Paleozoic appinite from the Appin district of the Scottish Caledonides [5] and appinite from the NW Iberian Massif, Spain [6]. In China, some appinites are also reported, e.g., the Permian appinite in the northern margin of the North China Craton [7] and Triassic appinite in northeastern China [8]. These appinites are generally coeval with high Ba-Sr granites, indicating mafic magma underplating events in collisional orogenic belts. The appinites are considered to be formed by the melting of the metasomatized mantle wedge in the post-collision stage, which may be caused by asthenospheric upwelling in the circumstances of slab break-off or slab roll-back [4]. The emplacement of appinitic magma beneath the continental crust would induce extensive crustal melting and granite formation [1,3]. Therefore, the genetic link between appinites and coeval granites provides a unique opportunity for tracing the nature of the mantle lithosphere and crust–mantle interaction in the convergent margin [3,4].

Triassic magmatism in the Qinling orogenic belt was considered to result from the collision process between the North China and Yangtze blocks [9–14]. Previous works mainly focus on the Triassic granites and associated mafic enclaves [10,12]. Some geodynamic models have been proposed, i.e., slab break-off [9,15], the melting of the delaminated lower crust in post-collisional setting [11] and the multi-stage melting of the subducted continental crust during the slow exhumation process [10,11]. However, the nature and melting mechanism of the mantle lithosphere, as well as its role in the formation of Triassic granites, still remain poorly understood.

The Triassic Laocheng appinite in the central Qinling section provides a unique opportunity to solve this problem. In this paper, we present new results of the chronology (zircon U-Pb dating), major and trace element geochemistry and in situ zircon Hf isotopic composition for Laocheng appinite. According to these new data, we discuss the following two important items: (1) the nature of the mantle lithosphere of the Qinling Orogenic Belt; (2) the melting mechanism of the mantle lithosphere and its role in the generation of Triassic granites.

2. Geological Background

The Qinling orogeny is one of the main orogens in East Asia [16], which extends WNW–ESE across central China [14]. Two Paleozoic suture zones (e.g., the Shangdan and Mianlve suture zones) in the Qinling orogenic belt preserve ocean-continental evolutionary history. The Shangdan suture zone is located between the North and South Qinling blocks, which represent the tectonic relic of the Paleozoic Shangdan ocean [14]. The Mianlue suture zone is located between the northern margin of the Yangtze block and South Qinling block [17]; ophiolite complex in the Mianlve suture zone has an ambiguous tectonic implication. The North Qinling terrane consists of middle Paleozoic migmatite complex and associated Paleozoic granites [14]; South Qinling consists of Late Paleozoic medium-grade metamorphic rocks [16] and Triassic granites [11]. South of the Mianlue suture is the northern margin of the Yangtze block (Figure 1a).

Due to the northern subduction of the Mian–Lve ocean, the Triassic collision between the Yangtze and North China blocks along the Qinling–Dabie orogen caused voluminous Triassic granites [11,14]. The Triassic granites in the Qinling orogen comprise an approximately 400 km-long granite belt across the Qinling orogenic belt (Figure 1). The origin of these granites remains controversial; most scholars argue that these granites were formed in post-collisional extensional setting, which may be related to slab break-off and lower crust delamination [9–12].

The Laocheng pluton locates to the east of the Triassic Wulong composite pluton, which covers an area of ~24 km^2 (Figure 1b). The Laocheng pluton intrudes into Neoproterozoic—Ordovician quartzite, Cambrian-Ordovician graphite-quartzite and Silurian micaceous quartzite. The appinite occurs as mafic blocks (varying from several meters in size) that are enclosed by Laocheng granite; some granitic veins can be observed in the appinite (Figure 2a). Eight appinite samples were selected from the Laocheng village, 10 km to the north of Ningshan City (Figure 1c). The appinite is medium–grained (Figure 2), and consists of euhedral hornblende (50%~60%) and plagioclase (20% to 25%; $An_{40–45}$) with minor quartz (<5%) and biotite (5%~10%). The euhedral hornblende grain has a large size of 1 to 3 cm; some plagioclase and quartz grains are enclosed by the hornblende (Figure 2b). Accessory minerals include zircon, apatite, allanite, clinozoisite and magnetite. Rod-like or euhedral prismatic apatite mainly occurs as inclusions in hornblende and plagioclase.

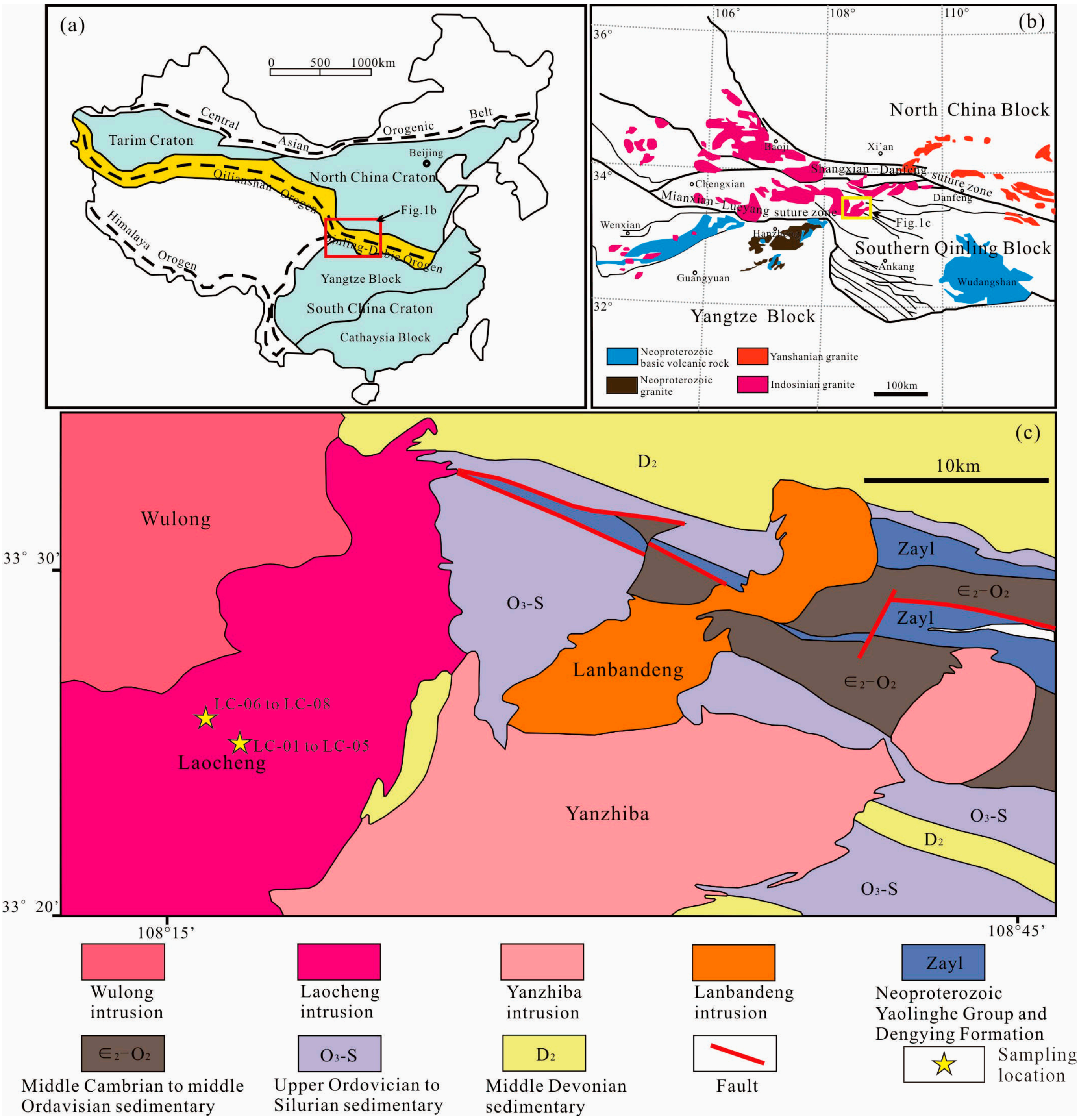

Figure 1. (**a**). Sketch Geological map of China, (**b**) geological map of the Qinling Orogenic belt and (**c**) the geological map of the Triassic Laocheng and Yanzhiba pluton.

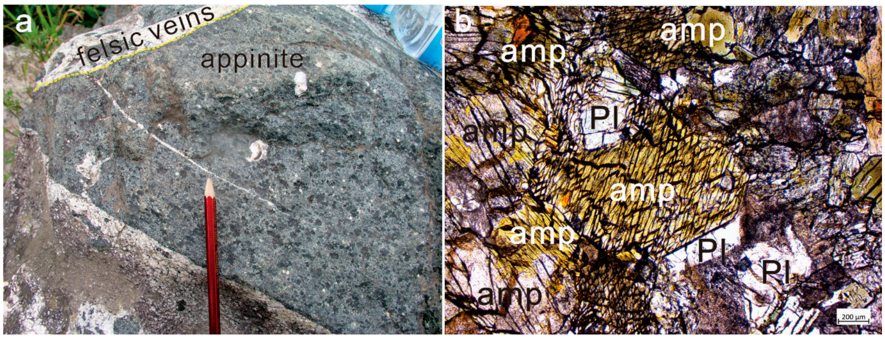

Figure 2. Field photo and microscope pictures for the appinite in the Laocheng pluton amp- amphibole; Bi-biotite; Kfs-K-feldspar; Pl-plagioclase; Qtz-quartz. (**a**) field photo of the Laocheng appinite; (**b**) microscope picture of the Laocheng appinite.

3. Analytical Methods

All analyses in this paper were performed at the State Key Laboratory of Continental Dynamics, Northwest University, China.

For bulk major- and trace-element analysis, fresh chips of whole rock samples were powdered to 200 mesh using a tungsten carbide ball mill. Major and trace elements were analyzed using XRF (Rikagu RIX 2100) and ICP–MS (Agilent 7700a), respectively. Analyses of USGS and Chinese national rock standards (BCR-2, GSR-1 and GSR-3) indicated that both analytical precision and accuracy for major elements were generally better than 5%. For trace element analysis, sample powders were digested using an HF+HNO_3 mixture in high-pressure Teflon bombs at 190 °C for 48 h, following the method of Liu et al. [18].

Laser ablation ICP–MS zircon U–Pb analyses were conducted on an Agilent 7700a ICP–MS equipped with a 193 nm laser, following the method of Yuan et al. [19]. The ion signal intensity ratio measured for both ^{238}U and ^{232}Th (NIST SRM 610) (^{238}U and ^{232}Th $\approx$ 1) was used as an indicator of complete vaporization [20]. These correction factors were then applied to each sample to correct for both instrumental mass bias and depth-dependent elemental and isotopic fractionation. Concentrations of U, Th, Pb and trace elements were calibrated by using ^{29}Si as an internal standard and NIST SRM 610 as an external standard. The two standard zircons 91500 and GJ-1 yielded weighted mean ^{206}Pb/^{238}U ages of 1064.2 ± 3.1 Ma (n = 14, 2σ) and 603.1 ± 3.4 Ma (n = 12, 2σ), respectively, which are in good agreement with the recommended ID-TIMS ages [20].

In situ zircon Hf isotopic analyses were conducted using a Nu Plasma HR multi-collector mass spectrometer, equipped with a 193 nm laser ablation sampling system. The ^{176}Yb/^{172}Yb value of 0.5887 and mean βYb value obtained during Hf analysis on the same spot were applied for the interference correction of ^{176}Yb on ^{176}Hf [21]. The notations of $\varepsilon_{Hf}(t)$ value, $f_{Lu/Hf}$, single-stage model age (T_{DM1}) and two-stage model age (T_{DM2}) were defined as in Yuan et al. [19].

4. Results

4.1. Zircon LA-ICP MS Dating

The zircon U-Th-Pb analysis results are listed in Supplementary Table S1. Zircons from the Laocheng appinite have a length of 100 to 200 μm, with respect ratios of 2:1 to 3:1; most grains display developed oscillatory zoning (Figure 3). Twenty-four analysis spots have high and variable U and Th contents (U = 197 to 815 ppm, Th = 211 to 9228 ppm), with variable Th/U ratios of 0.45 to 27.74. According to the U-Pb analysis results, two age groups are identified in the Laocheng appinite (Figure 4): the first group including 12 grains have older ^{206}Pb/^{238}U ages of 226 ± 4 Ma to 246 ± 5 Ma, with a weighted mean age of 233 ± 4 Ma (MSWD = 1.0, n = 12); this age is identical with the diorite from the margin of the Wulong pluton [11]. The younger group have ^{206}Pb/^{238}U ages of 212 ± 5 Ma to 221 ± 4 Ma, with a weighted mean age of 216 ± 3 Ma (MSWD = 0.85, n = 11). There are no obvious geochemical differences between the older and younger groups (Figure 5).

There are two possibilities to explain this age variation, e.g., the older group represent early magma pulse, or the older group represent captured grains. The younger ages are consistent with other Triassic granites and associated mafic enclaves in the Qinling Orogenic Belt [12,13,22], which is considered to represent the crystallization age of the Laocheng appinite.

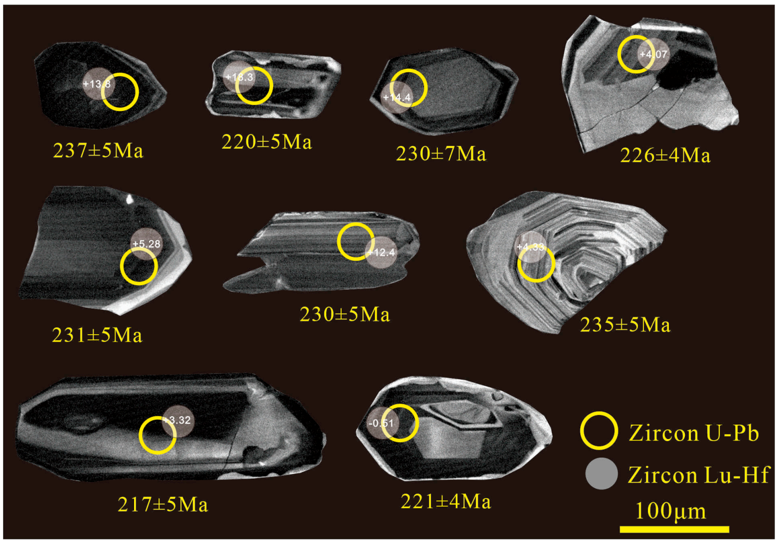

Figure 3. Cathodoluminescence (CL) images of typical zircons from the Laocheng appinite. Circles indicate the location of LA-MC-ICP MS Hf analyses; the numbers in circles refer to the $\varepsilon_{Hf}(t)$ values. All $\varepsilon_{Hf}(t)$ values of the granites were calculated according to their crystallization age.

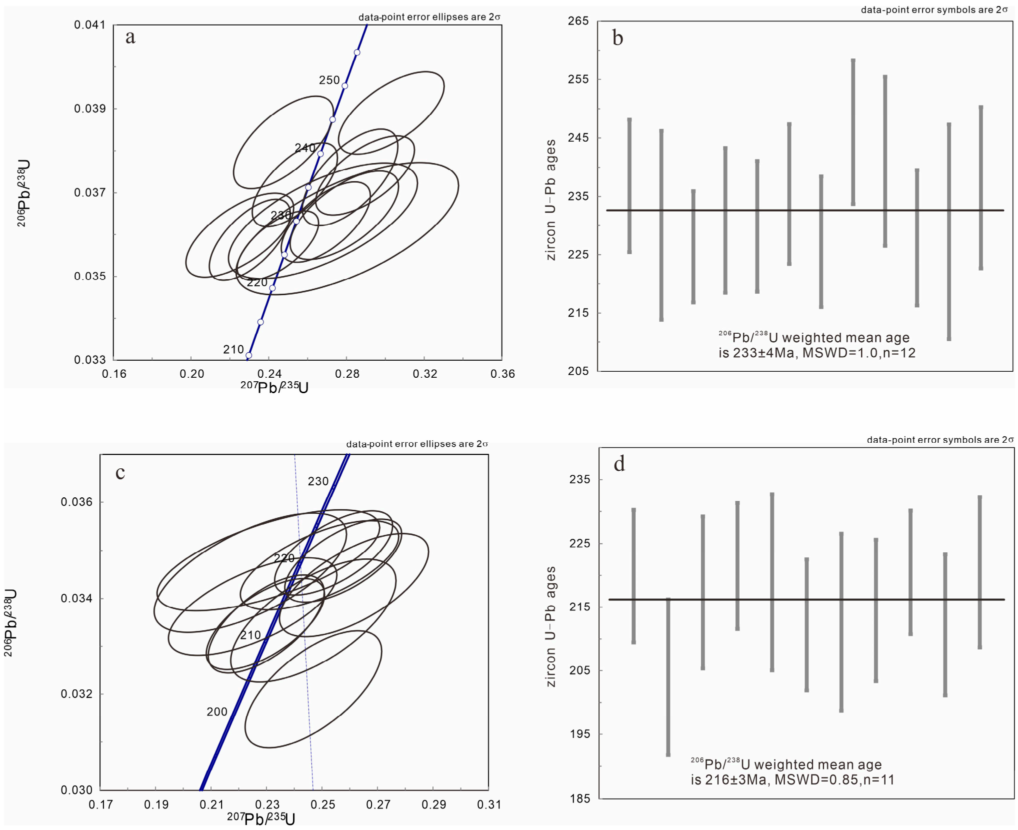

Figure 4. Zircon LA-ICP MS U-Pb concordia diagram (**a**,**c**) and weighted mean ages (**b**,**d**) for the Laocheng appinite.

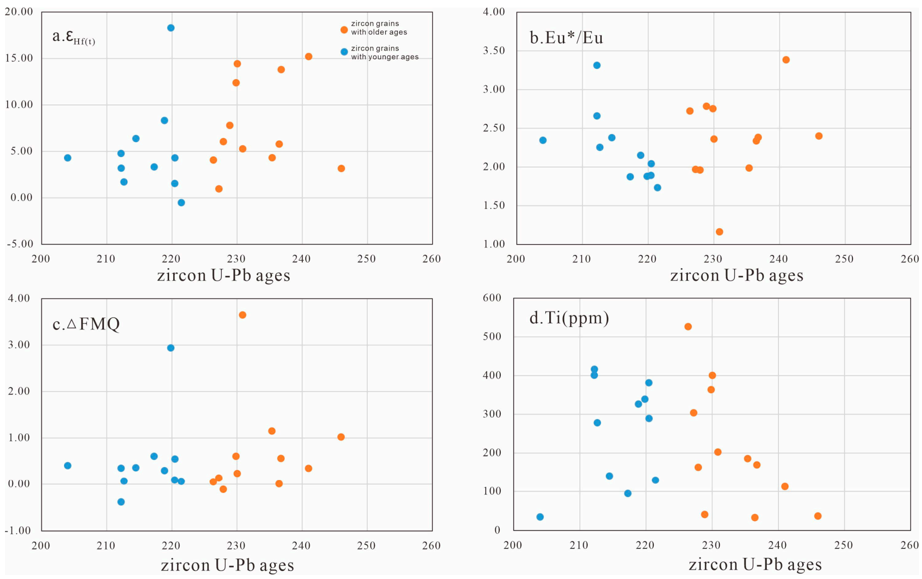

Figure 5. Zircon geochemical differences for the Laocheng appinite. Zircon U-Pb ages vs. $\varepsilon_{Hf}(t)$ (**a**), Eu*/Eu anomalies (**b**), △FMQ (**c**) and Ti contents (**d**) diagrams.

4.2. Major and Trace Element Geochemistry

The major and trace element compositions of the appinite are given in Table 1. The Laocheng appinite is magnesian, calc-alkaline and metaluminous (Figure 6a); it has SiO_2 = 46.55 to 50.44% and aluminous saturation index (A/CNK) values ranging from 0.42 to 0.67. It has low K_2O (0.83% to 2.37%) contents, with high Na_2O/K_2O ratios of 1.5 to 2.7, similar to those of the Cenozoic adakites that derived from the melting of the subducted oceanic crust [2] (Figure 6b). It has high MgO (7.62 to 10.76%) contents and Mg# (Mg# = Mg/(Mg + Fe) = 61 to 75), which is higher at given SiO_2 contents than the experimental melts derived from metabasites [2,23], similar to those of the sanukite in modern arcs [24,25].

Table 1. Bulk-rock geochemistry for the Laocheng appinite from Qinling.

Sample	LC-01	LC-02	LC-03	LC-06	LC-07	LC-08
SiO_2	46.55	50.16	50.24	50.21	50.38	50.44
TiO_2	2.33	0.74	0.73	0.74	0.74	0.73
Al_2O_3	15.59	11.91	12.61	11.74	11.99	12.18
Fe_2O_3T	11.48	8.19	8.27	8.39	8.21	8.31
MnO	0.15	0.13	0.13	0.14	0.13	0.13
MgO	7.62	10.56	10.09	10.76	10.47	10.58
CaO	8.16	13.29	13.03	13.11	12.52	13.15
Na_2O	3.61	1.93	2.27	1.94	2.28	1.89
K_2O	2.37	0.94	0.83	0.99	0.93	0.91
P_2O_5	0.76	0.16	0.17	0.18	0.18	0.17
LOI	1.73	1.56	1.13	1.58	1.68	1.58
TOTAL	100.35	99.57	99.5	99.78	99.51	100.07
Li	47.5	38.4	43.2	47	40.5	42.9
Be	0.78	0.7	0.75	0.74	0.86	0.74
Sc	30.1	30.5	33.5	31.6	30.7	33.6
V	193	190	184	191	186	194
Cr	650	672	599	680	623	677
Co	52.2	51.3	52.4	52.4	50.1	52.7
Ni	127	129	121	127	130	125
Cu	70.7	66.2	81.5	65.7	67.8	67.8
Zn	61.4	159	56.9	63.1	123	56.7
Ga	13.7	13.5	14.1	13.5	13.3	13.6

Table 1. *Cont.*

Sample	LC-01	LC-02	LC-03	LC-06	LC-07	LC-08
Ge	1.46	1.46	1.5	1.4	1.37	1.48
Rb	58.6	42.6	33.6	45.5	41.9	38.7
Sr	635	625	651	614	676	596
Y	17.1	17	17.4	17.3	16.7	17.5
Zr	72.2	69.7	64.9	70.3	69.2	69.1
Nb	4.17	4.03	4.41	4.1	3.99	4.21
Cs	2.98	2.72	2.4	3.06	2.19	2.58
Ba	347	340	311	350	334	332
La	15.6	15.5	15	15.7	15.4	15.6
Ce	34	34.3	34	34.4	33.8	34.3
Pr	4.4	4.41	4.45	4.47	4.34	4.48
Nd	18.9	19	19.1	19.4	18.8	19.5
Sm	3.95	4.01	4.03	4.04	3.93	4.09
Eu	1.17	1.17	1.17	1.18	1.15	1.19
Gd	3.8	3.83	3.85	3.89	3.79	3.93
Tb	0.55	0.55	0.56	0.57	0.55	0.57
Dy	3.28	3.32	3.31	3.41	3.28	3.45
Ho	0.64	0.64	0.65	0.66	0.64	0.66
Er	1.72	1.73	1.76	1.76	1.72	1.79
Tm	0.24	0.24	0.24	0.24	0.24	0.25
Yb	1.47	1.46	1.48	1.51	1.45	1.51
Lu	0.21	0.21	0.22	0.22	0.21	0.22
Hf	2	1.97	1.93	1.98	1.94	1.99
Ta	0.24	0.24	0.26	0.24	0.23	0.25
Pb	4.9	5.97	6.83	4.97	6.19	4.94
Th	1.92	1.83	1.46	1.94	1.76	1.8
U	0.55	0.45	0.48	0.46	0.51	0.49
Mg#	61	75	74	75	75	75
Eu/Eu*	0.93	0.91	0.91	0.91	0.91	0.91
ΣREE	90	90	90	91	89	92

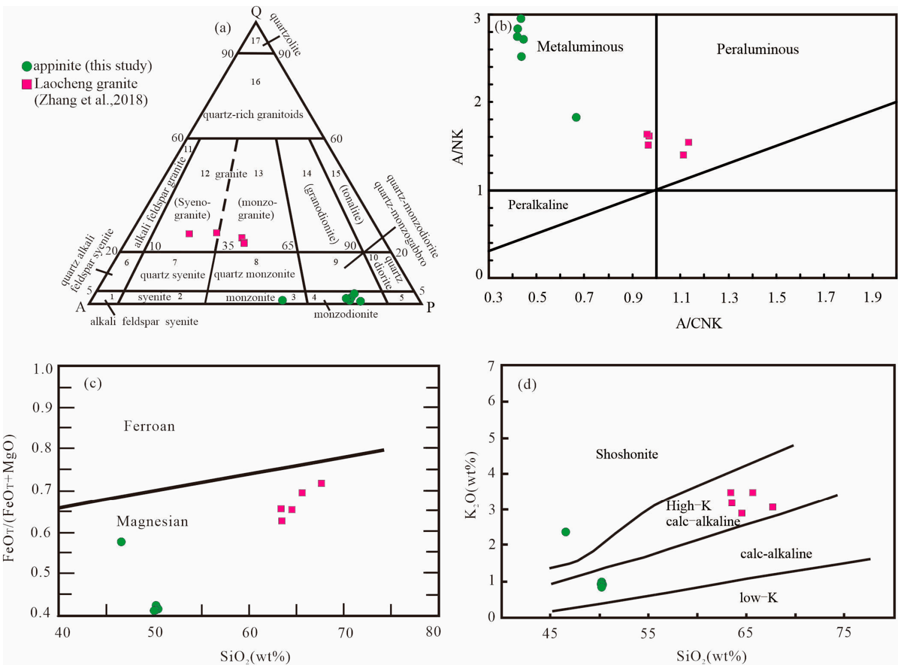

Figure 6. Plots of Q-A-P (**a**), A/NK [$Al_2O_3/(Na_2O + K_2O)$] vs. A/CNK (molar ratio $Al_2O_3/(CaO + Na_2O + K_2O)$); (**b**), SiO_2-FeO/(FeO + Mg) (**c**) and SiO_2-K_2O (**d**) diagrams for the Triassic Laocheng appinite. The data of the Laocheng granite was from Zhang et al. [26].

The Laocheng appinite displays high Sr (596 to 676 ppm) and low Y (16.7 to 17.4 ppm) contents, with moderate Sr/Y (34 to 40) and insignificant Eu anomalies (0.90 to 0.91). Unlike the high-Si adakite that derived from the melting of subducted slab [27,28], the Laocheng appinite display higher Cr (599 to 680 ppm), Ni (121 to 130 ppm) and Co (50.1 to 52.7 ppm) contents; this is identical to those of the sanukite [29] that formed by mantle wedge melting. Furthermore, it has high Nb/Ta ratios of 16.8 to 17.4. As shown in the chrondrite normalized REE patterns (Figure 7), the Laocheng display slight depletion in MREE; this is commonly attributed to the presence of residual hornblende in the source [30].

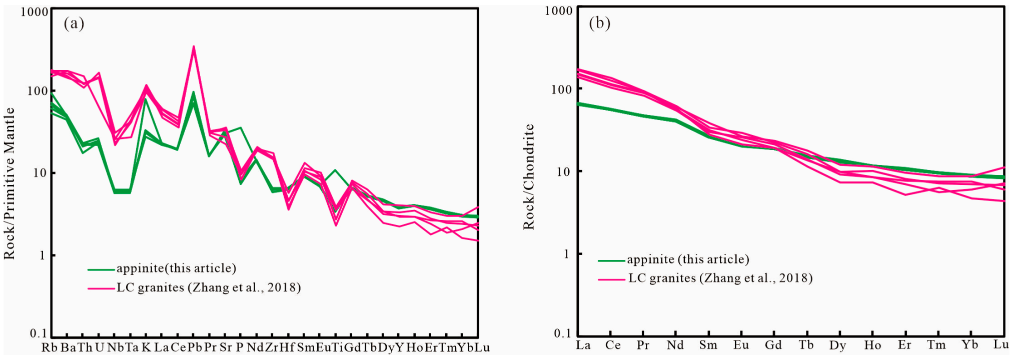

Figure 7. Chondrite-normalized REE patterns (**a**) and primitive mantle (PM) normalized trace element spider diagrams (**b**) for the Triassic Laocheng appinite. The data of the Laocheng granite was from Zhang et al. [26].

4.3. Zircon Lu-Hf Isotope, Trace Element and Oxygen Fugacity

Twenty-three Lu–Hf analyses spots were obtained from 23 grains (Supplementary Table S1). The initial Hf isotope ratios are calculated at t = 220 Ma. Zircons from the appinite displays extremely low $^{176}Lu/^{177}Hf$ ratios of 0.000396 to 0.001615, suggesting no radiogenic in growth of Hf over the ~220 Ma. Zircons from the appinite display depleted Lu-Hf isotopic compositions, they have $^{176}Hf/^{177}Hf$ ratios 0.282681 to 0.283158, with positive $\varepsilon_{Hf}(t)$ values of +0.97 to +18.21 (Figure 8), with corresponding crustal model ages of 341 to 1002 Ma, only one exception have negative $\varepsilon_{Hf}(t)$ values of −0.51. The predominant positive $\varepsilon_{Hf}(t)$ values suggesting a depleted source, this is clearly different from other Triassic granites and mafic enclaves in the Qinling orogenic belt [12,14].

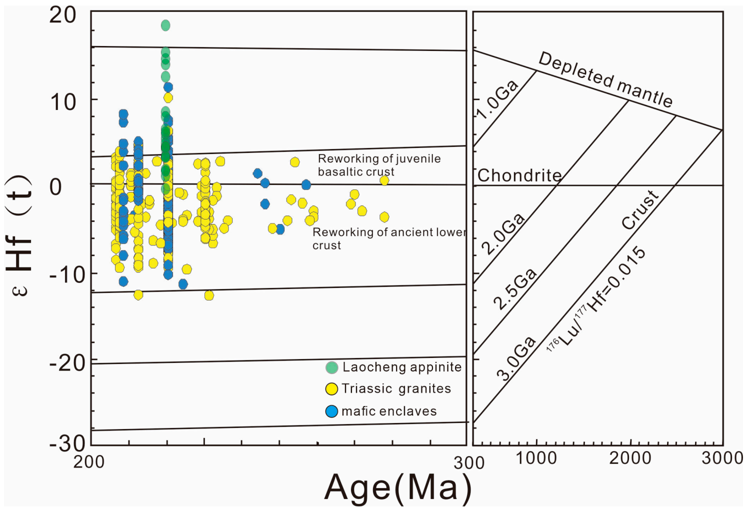

Figure 8. Age-corrected zircon $\varepsilon_{Hf}(t)$ vs. ages diagram for the zircons in Triassic granites, associated mafic enclaves and the Laocheng appinite in the Qinling orogenic belt. The Hf isotope ratios of the ancient crust basement are delimited by the 1.5 and 3.0 Ga juvenile crust evolution trends calculated assuming the $^{176}Lu/^{177}Hf$ of average continental crust (0.015).

Zircons in the appinite have positive Eu anomalies (Eu*/Eu = 1.16 to 1.39) and variable Ce anomalies (Ce*/Ce = 0.15 to 10.2). According to the trace element geochemistry, we have calculated the Ti-in zircon temperature and oxygen fugacity (Supplementary Table S1) for the zircons. The Ti-in zircon temperatures were calculated according to the method by Ferry and Watson [31], with log αSiO_2 = 1.0, log αTiO_2= 1.0. Zircon oxygen fugacity was calculated by method of Loucks et al. [31]. They have extremely high Ti-in zircon temperatures of 873 to 1333 °C (Supplementary Table S1). According to calculating results by the method of Loucks et al. [32], most of the zircons have log fO_2 = −3.35 to −12.16, with variable ΔFMQ values of 0 to +1 (Figure 5), these values are identical with the oxygen fugacity (ΔFMQ = +0.3 to +2.0) of the mantle wedge in subduction zone [33], indicating a relatively oxidizing condition.

5. Discussion

5.1. Hydrous Mafic Melts That Derived from Metasomatized Mantle Wedge

The appinites in orogenic belts are generally considered to be formed by the hydrous melting of the sub-arc mantle [4,8]. The Laocheng appinite has a basaltic composition, with low SiO_2 (46.55 to 50.44%) contents and high Cr (599 to 680 ppm), Ni (121 to 130 ppm) and Co (50.1 to 52.7 ppm) contents; these features are identical with the primitive melts that derived from the melting of the metasomatized mantle wedge [5]. Its depleted zircon Lu-Hf isotopic compositions ($\varepsilon_{Hf(t)}$ = +0.97 to +18.21) indicate a depleted mantle source. As shown in the Ba/La vs. Th/Yb discrimination diagram (Figure 9b), the Laocheng appinite displays low Th/Yb and Ba/La ratios. This is identical with the Setouchi sanukitiods in SW Japan [24], suggesting that sediment-derived fluid and melts are not the metasomatis agent.

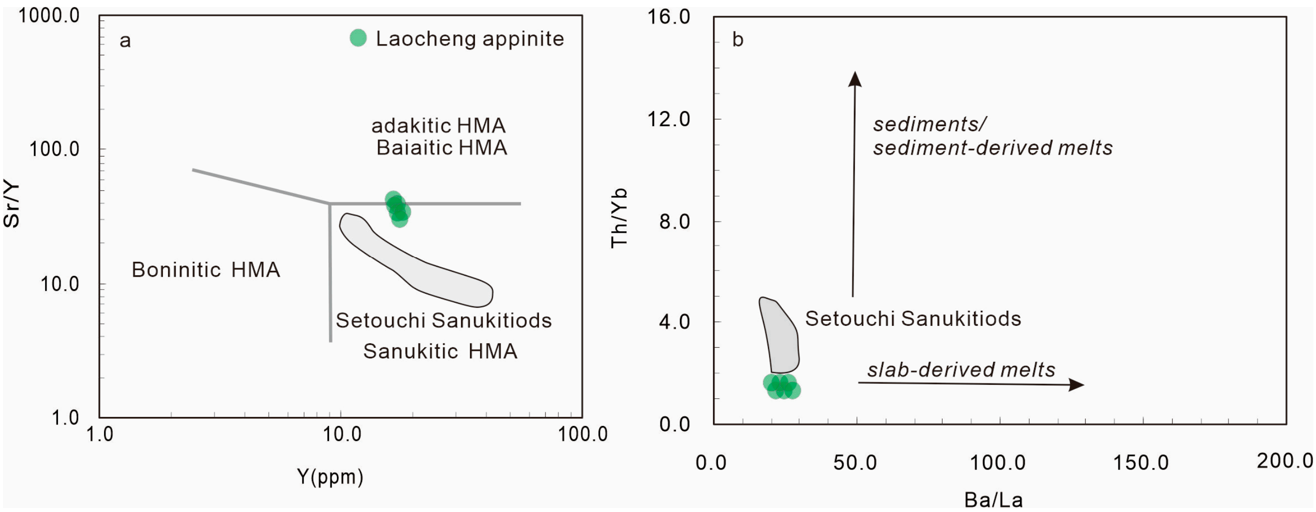

Figure 9. Y vs. Sr/Y (**a**) and Ba/La vs. Th/Yb (**b**) discrimination diagrams (after Tatsumi, 2006) for the Laocheng appinite [24].

The high abundance of euhedral hornblende in the appinite indicates a water-rich condition [5], in combination with its arc-like trace element geochemistry, i.e., enrichment in LREE and LILEs (e.g., Cs, Ba, K and Sr) and depletion in HSFEs (e.g., Nb, Ta and Ti) (Figure 7); these features are similar to those of appinite worldwide, e.g., Caledonide orogen [6], the Avalon Terrane of Nova Scotia, Canada [34], Central Gangdese, Tibet [35]. These features indicate that the hydrous mafic melts were derived from the melting of the sub-arc mantle wedge [4].

The Laocheng appinite display high Sr (596 to 676 ppm) and low Y (16.7 to 17.5 ppm < 18 ppm) contents, resulting in moderate Sr/Y ratios of 37 to 40; these features are identical with the sanukite that formed by the hydrous melting of the metasomatized mantle [27,29], which was previously metasomatized by slab-derived adakitic melts [5,36,37]. Furthermore, the zircons in the appinite display positive Eu anomalies (Eu*/Eu = 1.16 to 1.39) (Supplementary Table S1), which indicate the absence of plagiolcase residue in its source region [3,38]. The plagioclase may become unstable in the case of fluid-flux melting or high pressure (>1.2 Gpa) [3], while the high abundance of euhedral hornblende in the appinite indicates the water-rich feature of the appinite. In summary, we argue that the Laocheng appinite was probably derived from a hydrated depleted mantle source; the metasomatic agent may be derived from the dehydration of the subducted oceanic slab.

5.2. Crystallization Process and Relative High Oxygen Fugacity

The melting temperature and oxygen fugacity are the two main factors that control the melting reaction and melt geochemical properties [5]. According to the Ti-in zircon thermometer [30], zircons in the Laocheng appinite display extremely high temperatures of 873 to 1333 °C, with three exceptions below 1000 °C (Supplementary Table S1). The abundance of water in the mantle lithosphere has a significant effect on the stability of the amphibole and melting temperature [38]; limited H_2O (0.05 to 0.5%) in the metasomatized mantle would cause an amphibole dehydration (around 1100 °C, 1.5 to 3 GPa) melting event, which can produce some hydrous mafic melts [38]. The hornblende-rich mineralogical feature of the Laocheng appinite suggests a water-rich condition [4], while the high H_2O contents may originate from a hydrated mantle source [38] or result from a water-rich process in the late-stage magma crystallization [4].

In addition, zircons in the Laocheng appinite display high oxygen fugacity, according to results calculated by the method of Loucks et al. [32]; the zircons have $\log fO_2 = -3.35$ to -12.16, with ΔFMQ values ranging from 0 to +1.0, indicating an oxidized condition. In combination with the positive Eu anomalies (Eu*/Eu = 1.16 to 1.39) of the zircons, it suggests that the zircons that record high temperature and high oxygen fugacity are crystallized in the early crystallization stage. In summary, according to the zircon chemistry, we propose that the Laocheng appinite was formed by the high-temperature melting of the oxidized sub-arc mantle wedge.

5.3. Significance for the Granitic Magmatism and Magmatic Ore Deposits

The Laocheng appinite is of identical age with the Triassic granites in South Qinling [9–15], the northern margin of the Yangtze block [11,39] and western Qinling [38], indicating a close genetic link with Triassic granitic magmatism. Previous works on the coeval mafic enclaves that hosted the Triassic granites have suggested that the underplating of mafic magma induces extensive crustal melting and the formation of voluminous granites, which is generally attributed to either slab breakoff along the Qinling–Dabie orogen [9,10] or lower crust delamination into the asthenosphere mantle [12]. However, due to the complex magma mixing/mingling process, the mafic enclaves display ambiguous petrological and geochemical features, which makes it hard to trace the origin and melting condition of the mafic melt just according to the mafic enclaves [12,13].

Several lines of evidence approve the Late-Triassic post-collision setting in the Qinling orogenic belt; e.g., the occurrence of Late-Triassic Shahewan rapakivi-textured granites (210 Ma) indicate post-collision extension setting [40]. This is also approved by the coeval lamprophyre dykes [41] that intruded into the Shahewan pluton; this lamprophyre dyke has $^{40}Ar/^{39}Ar$ age of 209 ± 1.4 Ma; it is enriched in LILEs and LREE, with obvious depletion in Nb, Ta and Ti, in combination with their evolved Sr-Nd isotopic compositions. Wang et al. [41] proposed that this lamprophyre dyke was derived from the decompression melting of the metasomatized mantle in extensional setting.

As mentioned above, the Laocheng appinite display depleted zircon Lu-Hf isotopic compositions and extremely high Ti-in zircon temperatures in combination with abundant euhedral amphibole grains and high Mg# values; it is suggested that the Laocheng appinite represent primitive hydrous mafic melts that derived from the melting of the metasomatized mantle wedge [5]. In the circumstance of asthenosphere upwelling when subduction terminates (Figure 10), the extensive melting of the metasomatized mantle wedge would produce voluminous hydrous mafic melts that underplated beneath the base of the arc crust [5,6]. The underplating of this mafic melt would induce the hydrous melting of the lower crust in variable temperatures and cause voluminous coeval granites in the orogenic belts [6]. In summary, we suggest that the formation of Laocheng appinite has great significance for the genesis of the Triassic granites and associated metal deposits in the Qinling orogenic belt.

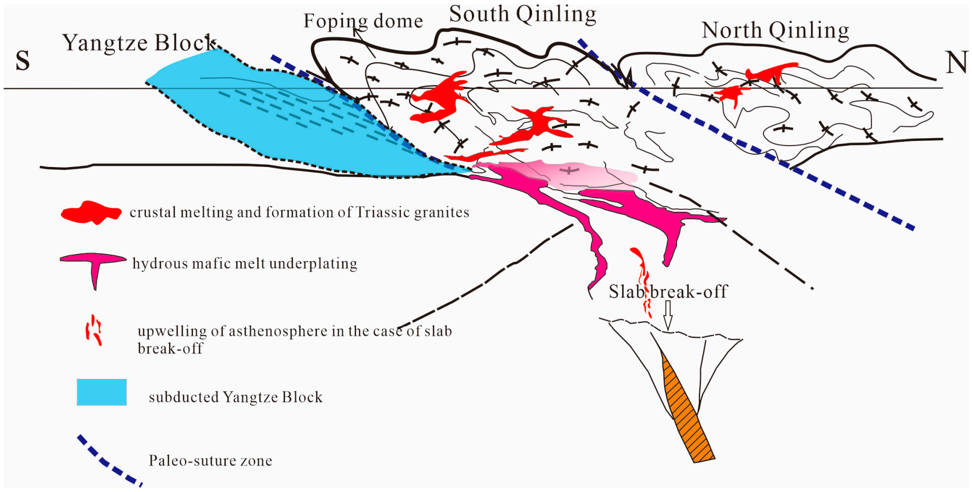

Figure 10. A simplified sketch tectonic cartoon model showing the formation of Triassic appinite and coeval granites in the Qinling orogenic belt.

6. Conclusions

(1) Laocheng appinite has an identical age to the Triassic granites in the Qinling orogenic belt, suggesting coeval mafic magma in the Qinling orogenic belt. Detailed whole-rock geochemistry and zircon chemistry indicate that the Laocheng appinite represent primitive hydrous mafic melts that derived from the melting of the depleted sub-arc mantle wedge.

(2) Zircons from the appinite display depleted Lu-Hf isotopic compositions, suggesting a depleted mantle source. Zircon chemistry also indicates a relative oxidizing condition. The underplating of this oxidizing, hydrous and high-temperature mafic melt beneath the base of the arc crust would induce the extensive melting of the lower crust and lead to the formation of voluminous Triassic granites and associated metal deposits in the Qinling orogenic belt.

Supplementary Materials: The following supporting information can be downloaded at: https://www.mdpi.com/article/10.3390/min13030441/s1, Table S1: Zircon U-Pb ages, Lu-Hf isotope and trace element for the Triassic Laocheng appinite.

Author Contributions: H.L. and H.G.: writing—original draft preparation, F.L. and Y.Z.: methodology, B.D.: data curation. All authors have read and agreed to the published version of the manuscript.

Funding: This research received no external funding.

Acknowledgments: We offer great thanks to the two anonymous reviewers; they provided us with many constructive comments helpful for improving the quality of our paper.

Conflicts of Interest: The authors declare that they have no conflict of interest.

References

1. Ducea, M.N.; Saleeby, J.B.; Bergantz, G. The Architecture, Chemistry, and Evolution of Continental Magmatic Arcs. *Annu. Rev. Earth Planet. Sci.* **2015**, *43*, 299–331. [CrossRef]
2. Wang, Q.; Hao, L.; Zhang, X.; Zhou, J.; Wang, J.; Li, Q.; Ma, L.; Zhang, L.; Qi, Y.; Tang, G.; et al. Adakitic rocks at convergent plate boundaries: Compositions and petrogenesis. *Sci. China Earth Sci.* **2020**, *63*, 1992–2016. [CrossRef]

3. Collins, W.J.; Murphy, J.B.; Johnson, T.E.; Huang, H.-Q. Critical role of water in the formation of continental crust. *Nat. Geosci.* **2020**, *13*, 331–338. [CrossRef]
4. Murphy, J.B. Appinite suites and their genetic relationship with coeval voluminous granitoid batholiths. *Int. Geol. Rev.* **2020**, *62*, 683–713. [CrossRef]
5. Murphy, J.B. Appinite suites: A record of the role of water in the genesis, transport, emplacement and crystallization of magma. *Earth-Sci. Rev.* **2013**, *119*, 35–59. [CrossRef]
6. Castro, A. Tonalite–granodiorite suites as cotectic systems: A review of experimental studies with applications to granitoid petrogenesis. *Earth-Sci. Rev.* **2013**, *124*, 68–95. [CrossRef]
7. Zhang, X.; Xue, F.; Yuan, L.; Ma, Y.; Wilde, S.A. Late Permian appinite–granite complex from northwestern Liaoning, North China Craton: Petrogenesis and tectonic implications. *Lithos* **2012**, *155*, 201–217. [CrossRef]
8. Zhao, C.; Qin, K.-Z.; Song, G.-X.; Li, G.-M.; Mao, J.-W. The Triassic Duobaoshan appinite-granite suite, NE China: Implications for a water-fluxed lithospheric mantle and an extensional setting related to the subduction of the Mongol-Okhotsk Ocean. *Lithos* **2021**, *394–395*, 106169. [CrossRef]
9. Sun, W.; Li, S.; Chen, Y.; Li, Y. Timing of synorogenic granitoids in the South Qinling, central China: Constraints on the evolution of the Qinling-Dabie orogenic belt. *J. Geol.* **2002**, *110*, 457–468. [CrossRef]
10. Qin, J.-F.; Lai, S.-C.; Grapes, R.; Diwu, C.-r.; Ju, Y.-J.; Li, Y.-F. Origin of LateTriassic high-Mg adakitic granitoid rocks from the Dongjiangkou area, Qinling orogen, central China: Implications for subduction of continental crust. *Lithos* **2010**, *120*, 347–367. [CrossRef]
11. Qin, J.-F.; Lai, S.-C.; Li, Y.-F. Multi-stage granitic magmatism during exhumation of subducted continental lithosphere: Evidence from the Wulong pluton, South Qinling. *Gondwana Res.* **2013**, *24*, 1108–1126. [CrossRef]
12. Qin, J.-F.; Lai, S.-C.; Long, X.-P.; Li, Y.-F.; Ju, Y.-J.; Zhao, S.-W.; Zhu, R.Z.; Wang, J.B.; Zhang, Z.Z. Hydrous melting of metasomatized mantle wedge and crustal growth in the post-collisional stage: Evidence from Late Triassic monzodiorite and its mafic enclaves in the south Qinling (central China). *Lithosphere* **2019**, *11*, 3–20. [CrossRef]
13. Hu, F.; Liu, S.; Ducea, M.N.; Zhang, W.; Deng, Z. The geochemical evolution of the granitoid rocks in the South Qinling Belt: Insights from the Dongjiangkou and Zhashui intrusions, central China. *Lithos* **2017**, *278–281*, 195–214. [CrossRef]
14. Dong, Y.; Sun, S.; Santosh, M.; Zhao, J.; Sun, J.; He, D.; Shi, X.; Hui, B.; Cheng, C.; Zhang, G. Central China Orogenic Belt and amalgamation of East Asian continents. *Gondwana Res.* **2021**, *100*, 131–194. [CrossRef]
15. Qin, J.; Lai, S.; Li, Y. Slab Breakoff Model for the Triassic Post-Collisional Adakitic Granitoids in the Qinling Orogen, Central China: Zircon U-Pb Ages, Geochemistry, and Sr-Nd-Pb Isotopic Constraints. *Int. Geol. Rev.* **2008**, *50*, 1080–1104. [CrossRef]
16. Mattauer, M.; Matte, P.; Malavieille, J.; Tapponnier, P.; Maluski, H.; Qin, X.Z.; Lun, L.Y.; Qin, T.Y. Tectonics of the Qinling Belt: Build-up and evolution of eastern Asia. *Nature* **1985**, *317*, 496–500. [CrossRef]
17. Lai, S.; Qin, J.; Chen, L.; Grapes, R. Geochemistry of ophiolites from the Mian-Lue suture zone: Implications for the tectonic evolution of the Qinling Orogen, central China. *Int. Geol. Rev.* **2008**, *50*, 650–664. [CrossRef]
18. Liu, Y.; Liu, X.; Hu, Z.; Diwu, C.; Yuan, H.; Gao, S. Evaluation of accuracy and long-term stability of determination of 37 trace elements in geological samples by ICP-MS. *Acta Petrol. Sin.* **2007**, *23*, 1203–1210.
19. Yuan, H.-L.; Gao, S.; Dai, M.-N.; Zong, C.-L.; Günther, D.; Fontaine, G.H.; Liu, X.M.; Diwu, C. Simultaneous determinations of U–Pb age, Hf isotopes and trace element compositions of zircon by excimer laser-ablation quadrupole and multiple-collector ICP-MS. *Chem. Geol.* **2008**, *247*, 100–118. [CrossRef]
20. Günther, D.; Hattendorf, B. Solid sample analysis using laser ablation inductively coupled plasma mass spectrometry. *TrAC Trends Anal. Chem.* **2005**, *24*, 255–265. [CrossRef]
21. Goolaerts, A.; Mattielli, N.; de Jong, J.; Weis, D.; Scoates, J.S. Hf and Lu isotopic reference values for the zircon standard 91500 by MC-ICP-MS. *Chem. Geol.* **2004**, *206*, 1–9. [CrossRef]
22. Lu, Y.-H.; Zhao, Z.-F.; Zheng, Y.-F. Geochemical constraints on the source nature and melting conditions of Triassic granites from South Qinling in central China. *Lithos* **2016**, *264*, 141–157. [CrossRef]
23. Rapp, R.P.; Shimizu, N.; Norman, M.D.; Applegate, G.S. Reaction between slab-derived melts and peridotite in the mantle wedge: Experimental constraints at 3.8 GPa. *Chem. Geol.* **1999**, *160*, 335–356. [CrossRef]
24. Tatsumi, Y.; Suzuki, T.; Kawabata, H.; Sato, K.; Miyazaki, T.; Chang, Q.; Takahashi, T.; Tani, K.; Shibata, T.; Yoshikawa, M. The Petrology and Geochemistry of Oto-Zan Composite Lava Flow on Shodo-Shima Island, SW Japan: Remelting of a Solidified High-Mg Andesite Magma. *J. Petrol.* **2006**, *47*, 595–629. [CrossRef]
25. Lu, Y.-J.; Loucks, R.R.; Fiorentini, M.L.; Yang, Z.-M.; Hou, Z.-Q. Fluid flux melting generated post-collisional high Sr/Y copper ore–forming water-rich magmas in Tibet. *Geology* **2015**, *43*, 583–586. [CrossRef]
26. Zhang, H.; Xiao, L.; Zhang, L.; Yuan, H.; Jin, L. Geochemical and Pb-Sr-Nd isotopic compositions of Indosinian granitoids from the Bikou block, northwest of the Yangtze plate: Constraints on petrogenesis, nature of deep crust and geodynamics. *Sci. China Ser. D Earth Sci.* **2007**, *50*, 972–983. [CrossRef]
27. Moyen, J.-F.; Martin, H. Forty years of TTG research. *Lithos* **2012**, *148*, 312–336. [CrossRef]
28. Defant, M.J. Derivation of some modern arc magmas by melting of young subducted lithosphere. *Nature* **1990**, *347*, 662–665. [CrossRef]
29. Martin, H.; Smithies, R.H.; Rapp, R.; Moyen, J.F.; Champion, D. An overview of adakite, tonalite–trondhjemite–granodiorite (TTG), and sanukitoid: Relationships and some implications for crustal evolution. *Lithos* **2005**, *79*, 1–24. [CrossRef]

30. Gromet, P.; Silver, L.T. REE Variations Across the Peninsular Ranges Batholith: Implications for Batholithic Petrogenesis and Crustal Growth in Magmatic Arcs. *J. Petrol.* **1987**, *28*, 75–125. [CrossRef]
31. Ferry, J.M.; Watson, E.B. New thermodynamic models and revised calibrations for the Ti-in-zircon and Zr-in-rutile thermometers. *Contrib. Mineral. Petrol.* **2007**, *154*, 429–437. [CrossRef]
32. Loucks, R.R.; Fiorentini, M.L.; Henríquez, G.J. New Magmatic Oxybarometer Using Trace Elements in Zircon. *J. Petrol.* **2020**, *61*, egaa034. [CrossRef]
33. Parkinson, I.J.; Arculus, R.J. The redox state of subduction zones: Insights from arc-peridotites. *Chem. Geol.* **1999**, *160*, 409–423. [CrossRef]
34. Pe-Piper, G.; Piper, D.J. The Jeffers Brook diorite–granodiorite pluton: Style of emplacement and role of volatiles at various crustal levels in Avalonian appinites, Canadian Appalachians. *Int. J. Earth Sci.* **2018**, *107*, 863–883. [CrossRef]
35. Meng, Y.; Xu, Z.; Santosh, M.; Ma, X.; Chen, X.; Guo, G.; Liu, F. Late Triassic crustal growth in southern Tibet: Evidence from the Gangdese magmatic belt. *Gondwana Res.* **2016**, *37*, 449–464. [CrossRef]
36. Kiseeva, E.S.; Kamenetsky, V.S.; Yaxley, G.M.; Shee, S.R. Mantle melting versus mantle metasomatism–"The chicken or the egg" dilemma. *Chem. Geol.* **2017**, *455*, 120–130. [CrossRef]
37. Cashman, K.V.; Edmonds, M. Mafic glass compositions: A record of magma storage conditions, mixing and ascent. *Philos. Trans. R. Soc. A Math. Phys. Eng. Sci.* **2019**, *377*, 20180004. [CrossRef]
38. Mandler, B.E.; Grove, T.L. Controls on the stability and composition of amphibole in the Earth's mantle. *Contrib. Mineral. Petrol.* **2016**, *171*, 1–20. [CrossRef]
39. Tang, M.; Ji, W.-Q.; Chu, X.; Wu, A.; Chen, C. Reconstructing crustal thickness evolution from europium anomalies in detrital zircons. *Geology* **2020**, *49*, 76–80. [CrossRef]
40. Wang, X.; Wang, T.; Castro, A.; Pedreira, R.; Lu, X.; Xiao, Q. Triassic granitoids of the Qinling orogen, central China: Genetic relationship of enclaves and rapakivi-textured rocks. *Lithos* **2011**, *126*, 369–387. [CrossRef]
41. Wang, F.; Lu, X.-X.; Lo, C.-H.; Wu, F.-Y.; He, H.-Y.; Yang, L.-K.; Zhu, R.X. Post-collisional, potassic monzonite–minette complex (Shahewan) in the Qinling Mountains (central China): $^{40}Ar/^{39}Ar$ thermochronology, petrogenesis, and implications for the dynamic setting of the Qinling orogen. *J. Asian Earth Sci.* **2007**, *31*, 153–166. [CrossRef]